Development of a Cast Modular Connector for Seismic-Resistant Steel Moment Frames Part 1: Prototype Development

ALI SUMER, ROBERT B. FLEISCHMAN, and BLAKE E. HOSKISSON

A modular connector (MC) has been developed for use as an energy dissipating detail in seismic-resistant steel moment frames. The MC (see Figure 1) is a cast steel piece specially configured to provide reliable and consistent seismic performance, and serves as a bolted alternative to several new cast forms(modular nodes) being developed for welded construction (Fleischman, Sumer, and Li, 2002). These modular forms consider seismic performance requirements as a first step in design, prior to establishing the connection configuration. The impetus for developing the modular connections was the discovered susceptibility of welded beam-to-column connections in steel special moment frames (SMFs) to fracture during earthquakes (Malley, 1998). The poor performance of the SMFs has led to major revisions in the design and construction of welded connections (FEMA, 2000a) and also a renewed interest in bolted connections (FEMA, 2000b). The MC is one such bolted connection specially made for seismic performance.

The MC provides reliable and repeatable seismic performance through a configuration specifically engineered for superior ductility and energy dissipation. The geometries required to accomplish this goal are not readily available with traditional rolled shapes. Thus, the MC designs (as well as the modular node designs) rely on the versatility afforded by the casting process to engineer an optimal geometric configuration for seismic performance. This approach is in contrast to the traditional practice of attempting to join main members directly or with arrangements of other rolled shapes (detail material). The designs further rely on advancements in casting technology to ensure that the connector possesses the required strength and ductility.

This paper describes the analytical development of a working prototype design for the MC. This stage of the development process involved a comprehensive program including: interdisciplinary industry meetings at the conceptual stages, extensive analytical research, castability, and constructability studies. A companion paper (Sumer, Fleischman, and Palmer, 2007) describes the prototyping and experimental verification of the MC Beta design. In both the analytical development and the experimental verification the focus is on the connector itself (with future work to examine overall connection behavior). Lessons were learned from an unsuccessful Alpha prototype that influenced and directed the designs for the later version. The result is a second generation (Beta) MC prototype that exhibits exceptional seismic performance in analytical simulations of isolated connectors including high-energy dissipation, ductility, and repeatability.

MODULAR CONNECTOR

The MC connects the beam flange to the column. Typical construction will involve shop welding or bolting the MC to the beam and field bolting the MC to the column (see Figure 2). The MC is thus identical in position and similar in form to structural tee (WT) sections (AISC, 2001) used

Ali Sumer is research assistant, department of civil and engineering mechanics, University of Arizona, Tucson, AZ.

Robert B. Fleischman is assistant professor, department of civil and engineering mechanics, University of Arizona, Tucson, AZ.

Blake E. Hoskisson is project engineer, Sure Steel Inc., Sandy, UT.

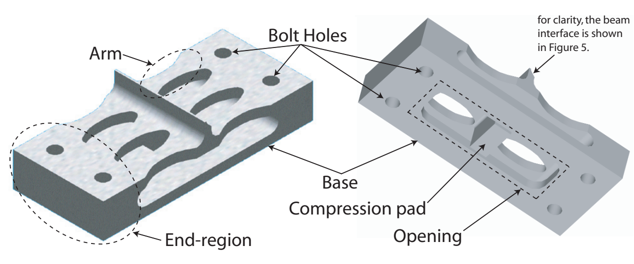

Fig. 1. Modular connector (MC) Beta prototype.

in traditional semi- or fully-rigid bolted T-stub connections (Swanson and Leon, 2000). However, the MC configuration contains two major differences that distinguish it from a WT: (1) a series of variable cross-section "arm" elements; and (2) end-regions connected by a base (refer to Figure 1). These features virtually eliminate high plastic strain demand and bolt prying forces, thereby producing superior energy dissipation and cyclic ductility characteristics, and are described in more detail as follows:

1. Arm elements: The intent of the MC design is to develop the ductility within the connector itself, an objective accomplished through stable yielding of arm elements. The use of the term "stable" here refers to the ability of these arm elements to undergo repeated plastic deformation cycles without loss of strength due to tearing, fracture or buckling. These arm elements possess variable cross-sections that produce a plastic zone distributed along the entire length of the element. Such a distribution reduces the intensity of strain concentrations that would occur, for instance, with the uniform section of a structural tee. This approach has been used successfully in various metal dampers used primarily for bracing systems (Whittaker, Bertero, Thompson, and Alonso, 1989), in other words, "Added Damping and Stiffness Plate Elements" (ADAS) (see Background). However, a different geometry is required for the MC application (Fleischman and Sumer, 2006) as will be summarized in the paper. The elimination of plastic strain concentrations permits the MC to more reliably survive large seismic events.

2. End-region: The end-region is configured to eliminate prying, thereby significantly reducing the forces that would otherwise develop in the bolts when the MC is subjected to axial tension from the beam flange. Reduction of force demands on the bolt is desirable from a capacity design standpoint (Astaneh, 1995). Of several end-region configurations considered (shown later in Figure 16), the base configuration indicated in Figure 1 emerged as the most effective and was incorporated into the MC prototype. The base eliminates prying by providing an alternate load path for the bending forces that typically "pry" the bolts at each end of a flange connector. Instead, a set of self-equilibrating forces are developed that cancel out in the connector, permitting the fasteners to carry axial force alone (see "Evaluation of End-Regions"). The incorporation of features to eliminate prying is key for the MC because in relying on long arm elements for ductility, a large eccentricity is created between the beam flange and column bolts. Such eccentricity would produce significant prying forces in a traditional connection (Nair, Birkemoe, and Munse, 1974).

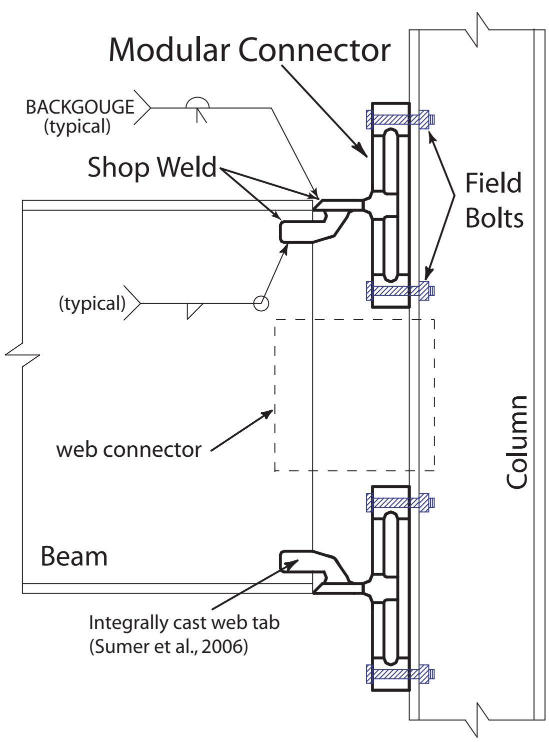

Fig.2. Schematic of beam-to-column connection using MCs.

BACKGROUND

Bolted rigid moment connections for SMFs (Special Moment Frames) (Popov and Takhirov, 2002) and bolted semi-rigid connections for partially restrained frames (Maison, Rex, Lindsey, and Kasai, 2000) have been investigated as alternatives to welded moment frames (Leon, Swanson, and Smallidge, 1999). The MC is a modified version of a bolted semi-rigid connection, the T-Stub, using casting technology to produce a series of variable section arm elements. These elements share the concept used in certain metal dampers (the ADAS device), but are configured differently due to changes in the application, in particular the presence of significant catenary forces. Background on bolted T-Stubs, ADAS devices, and the steel casting process is presented in the following paragraphs.

Bolted T-Stub Connections

The T-stub connection is comprised of a pair of WT sections connected by bolts at the beam flanges and bolted to the column. For seismic applications, the connection can be designed as a force-based detail, in other words, made stronger than the beam through a capacity design, thus forcing the plastic hinge into the beam (FEMA, 1999). Conversely, the connection pieces themselves can be used as the energy dissipating detail to develop the ductility. In the latter approach, energy dissipation in the T-stub detail will occur through concentrated plastic hinges forming in the tee flange sections adjacent to the bolt head and the tee stem (Piluso, Faella, and Rizzano, 2001) and tensile yielding of the tee stem (Leon et al., 1999). Regardless of the approach, the eccentricity between the tee stem and the column bolts will cause prying forces (*Q*) to develop (AISC, 2001) as shown in Figure 3. These prying forces amplify the axial force in the bolt and also create flexure in the bolt (Nair et al., 1974). Prying forces are often sufficient to require bolt sizes that are impractical for connections carrying large moments such as would occur in high seismic zones, or may also render the bolt the critical component. Frictional resistance of high strength bolts during slip affects hysteretic behavior of the connection (Roeder, Leon, and Preece, 1994). Therefore, prying actions can lead to less efficient energy dissipation from slippage due to successive losses in pretension.

Added Damping and Stiffness Plate Elements (ADAS)

Various metallic plate damper designs have been proposed as passive energy devices over the past two decades. Triangular plate devices developed in New Zealand (Tyler, 1978) were extended for use as piping support elements (Steimer, Godden, and Kelly, 1981). X-shaped plates, modified from the triangular plate devices, have been used as an energy-dissipating component of base isolation systems (Steimer and Chow, 1984). More recently, researchers (Whittaker et al., 1989) investigated the use of metal dampers to increase the energy dissipation capacity of conventional steel braced frames. These dampers, termed ADAS devices consisted of X-shaped ASTM A36 steel plates (see Figure 4a) bolted together at each end to approach fixed boundaries (see Figure 4b). The ADAS devices are oriented relative to the braces in the element's weak axis (see Figure 4c) to efficiently spread the inelastic demand of reverse curvature flexure. Tests performed by Bergman and Goel (1987) and Aiken, Nims, Whittaker, and James (1993) showed that ADAS elements can safely be designed for displacement ranges up to about 10 times yield displacement.

Steel Castings and the Steel Casting Process

Steel castings find widespread use as structural components in heavy industry applications that are safety critical, performance demanding (often subject to impact or sustained pressure) and in harsh environments (Monroe, 1995).

Steel foundries produce steel castings ranging from a few pounds to several tons. Figure 5 shows the casting of the MC Alpha prototype. The castings are created by pouring molten steel into molds (see Figure 5a). These molds are made by the joining of two opposing parts, typically a resin coated sand (1% phenolic urethane base) formed around a wood pattern of the cast piece (see Figure 5b). Internal features such as cavities are formed by placing solid parts, referred to as cores, within the molds (see Figure 5c).

Similar material to rolled steel (in terms of chemical composition and mechanical properties) can be cast, though castings do not receive the benefits of cold working associated with the rolling process. Instead, cast steel is isotropic with properties typically falling between the longitudinal and transverse properties of rolled steel (SFSA, 1995). However these properties only represent the quality of the steel, and not necessarily the quality of the casting itself. A further

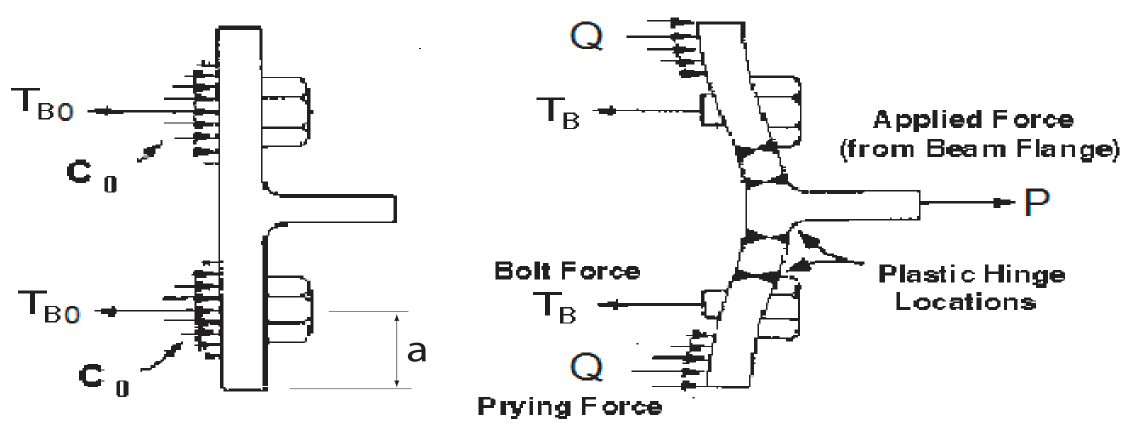

Fig. 3. Bolted T-stub: prying forces and plastic hinge locations.

requirement is that the casting has to be sound. Casting integrity is determined by solidification conditions that are heavily influenced by piece shape, size and wall thickness. In this regard, an essential feature of the casting process is the compensation of volumetric contraction in the cast piece during cooling to avoid internal shrinkage cavities. This objective is achieved by the strategic placement of a number of gravity-driven liquid feed metal reservoirs within the mold, referred to as risers (see Figure 5d). Quality control measures include mechanical testing, chemical spectrography, and nondestructive evaluation.

A major challenge in developing the physical prototype for the MC is to create a configuration that meets the seismic performance requirements and at the same time can be reliably cast, as discussed in the companion paper (Sumer et al., 2007).

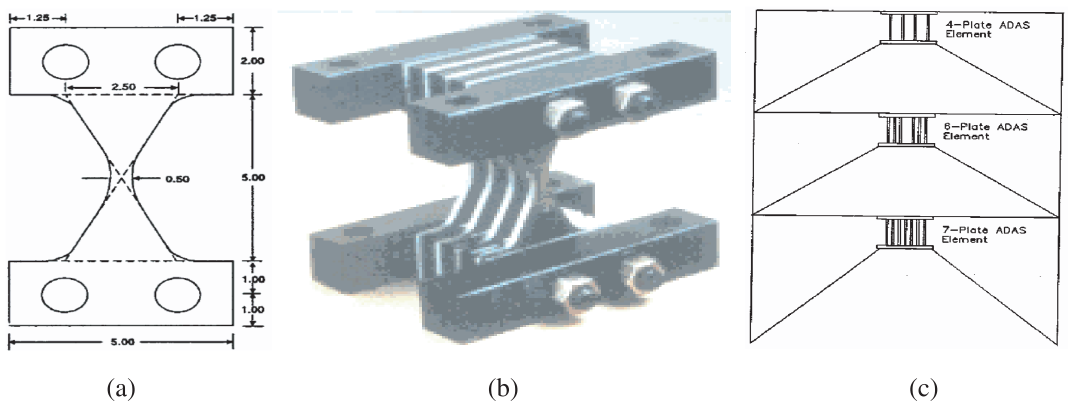

Fig. 4. (a) ADAS dimensions (in inches), (b) ADAS photo, and (c) schematic showing placement of ADAS device in seismic bracing (after Aiken et al., 1993).

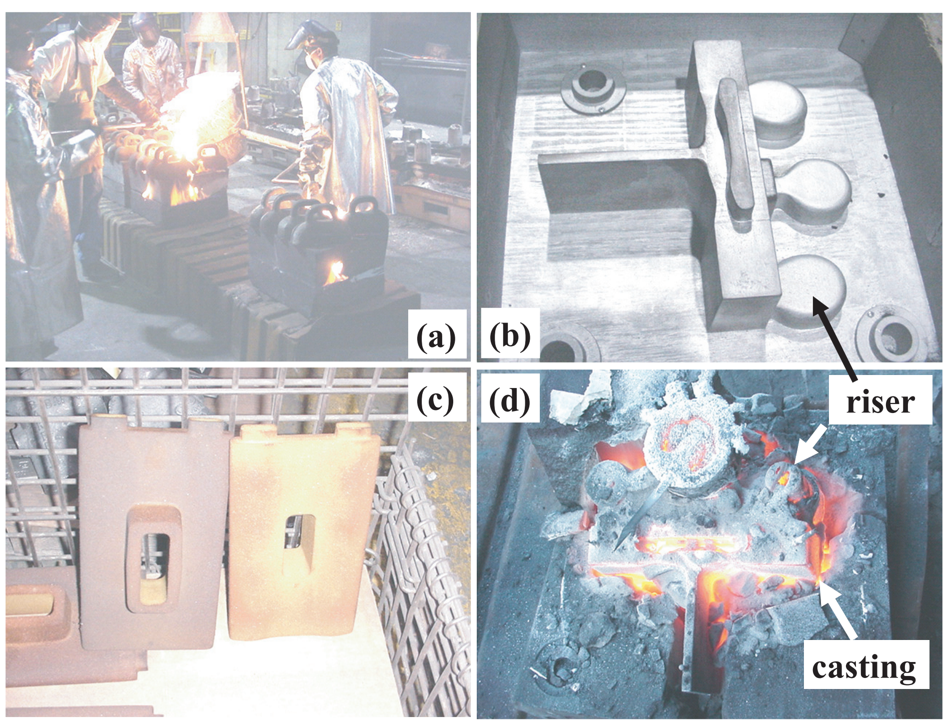

Fig. 5. MC casting: (a) filling the mold; (b) pattern; (c) cores; (d) cooling stage.

PROGRAM TO DEVELOP MODULAR CONNECTOR (MC) PROTOTYPE

The modular connector (MC) prototype was developed through an analytical research program and verified by an experimental research program (Sumer et al., 2007). Given that the form of the MC was entirely undefined at the initiation of the research, it was determined essential that the development process limit its focus to the component response of isolated connectors rather than starting with overall connection behavior. A simplified representation of connection mechanics (see Figure 6) is used to interpret the results of the analyses in this stage. Beam end moments are approximated as a tension-compression couple transfer through the beam flanges ($T_{bm} \cong M_{bm}/d_{bm}$); the beam end relative rotation (θ_{conn}) can be related to the MC displacement by assuming rotation about the opposing flange ($\Delta = \theta_{conn} d_{bm}$). The web connection contribution to flexure is ignored in this representation, and is assumed to carry only the (entire) shear force (see Figure 6). For the simplified representation, the load at the MC stem ($P \cong T_{bm}$) is applied perpendicular to the column face, as is the axial deflection Δ (see inset in Figure 6).

The isolated connector loading is a simplification of actual conditions. However, the examination of isolated specimens allowed economical and rapid evaluation of parameters for development of the MC prototype. The adequacy of these approximations was evaluated in a limited number of analyses of the full connection and was shown to be acceptable (Sumer, 2002).

The primary objective of the MC design is to provide reliable connection plastic rotation capacity. For this purpose, a limit of useful (monotonic) connection rotation was chosen at 0.05 radian. This value differs from the accepted cyclic ductility requirement of 0.04 radian in Appendix S of the AISC *Seismic Provisions for Structural Steel Buildings* (AISC, 2005) for reasons that are elucidated in the companion paper (Sumer et al., 2007). The connector displacement corresponding to this rotation is a beam-depth dependent quantity. For the purpose of evaluating features for the MC design, transformations in this paper are referenced to a 30-in.-deep beam. Thus, the deflection used to evaluate the MC is 0.05×30 in. = 1.5 in. Designs are evaluated by examining the maximum plastic strain at this "useful limit" displacement demand. Because the plastic strain field is two- or three-dimensional, the plastic strain components must be combined into a single scalar to allow comparison with an allowable value. In this paper, a function of plastic strains in the principal directions, termed von Mises or "equivalent plastic" strain (ANSYS, 2003), is used for this comparison.

The analytical program involved extensive nonlinear finite element (FE) analysis. Two-dimensional finite element (2D-FE) models were used to rapidly evaluate parameters and develop the basic form of the prototypes. Three dimensional finite element (3D-FE) solid models were used for verification of the 2D-FE models, stability examinations, castability analyses, and experimental predictions using the final prototype.

Alpha Prototype

The first generation MC design, or Alpha prototype (Fleischman and Hoskisson, 2000) possessed a variable section created through a thickness reduction termed an "hourglass" arm (see Figure 7). This prototype design was ultimately abandoned and therefore is not the focus of this paper, but some brief comments on its performance may be helpful to understand choices made in the MC Beta prototype design.

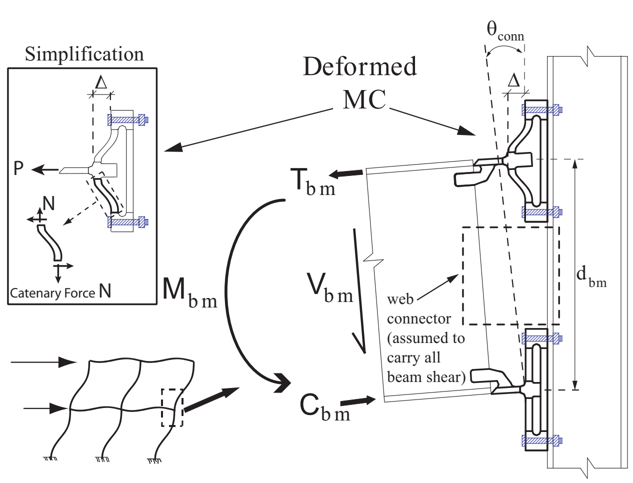

Fig. 6. Simplified representation of MC connection under beam moment.

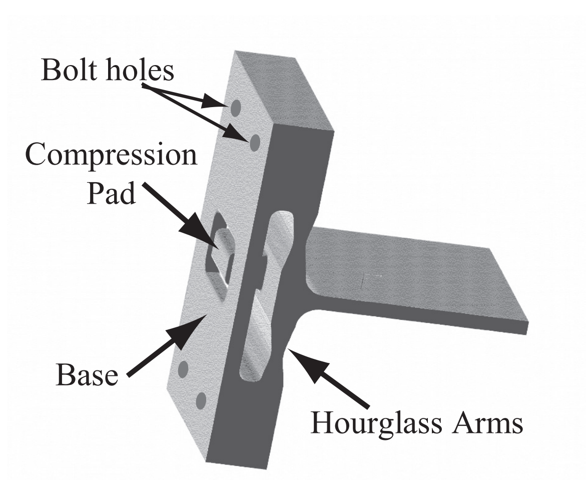

Fig. 7. Alpha prototype features.

Equivalent plastic strain contours of a half-symmetry model of an isolated Alpha prototype and a comparable WT (T-stub detail piece) at identical deformation demand are shown in Figure 8. In these small deflection theory analyses, the Alpha prototype exhibited the desired behavior as evidenced in the spread of the plastic zone causing lower plastic strain in the MC in comparison to the WT, and the stiffness of the base creates significantly lower plastic strain in the bolt threads and no plastic behavior in the bolt shank (Hoskisson, 2000).

However, the Alpha prototype did not exhibit the expected ductility in experiments (Hoskisson, 2000). The casting was cycled 13 times at an amplitude of only 0.4 in. (or 0.013 radian for a 30-in.-deep beam) prior to a low-cycle fatigue failure at the end of the arm (see Figure 9).

The unsuccessful performance of the Alpha prototype was primarily due to two factors: (1) castability issues associated with creating the physical prototype, as discussed in the companion paper (Sumer et al., 2007); and (2) the underestimation of the importance of catenary action, as described next.

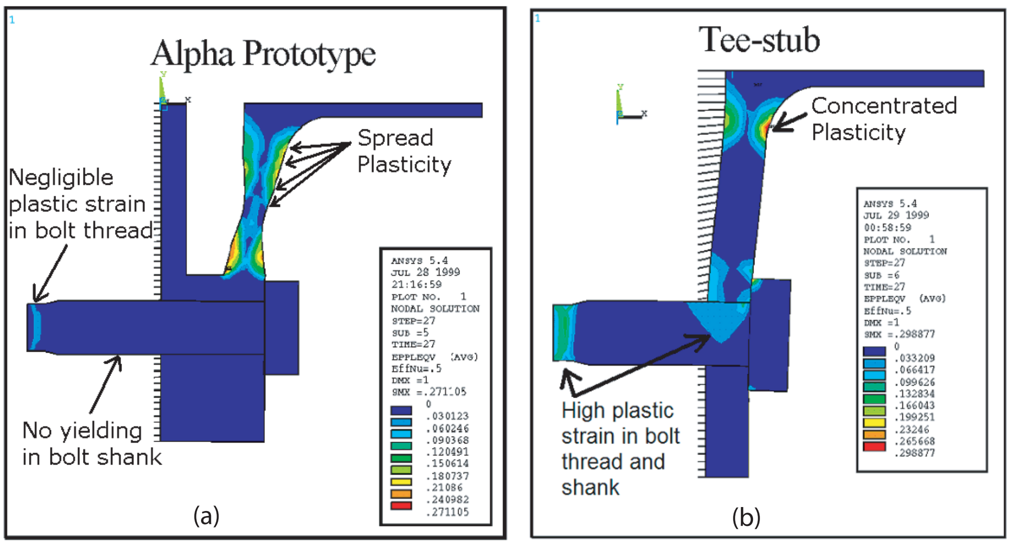

Fig. 8. Plastic strain demand comparison: (a) alpha prototype; and (b) tee-stub.

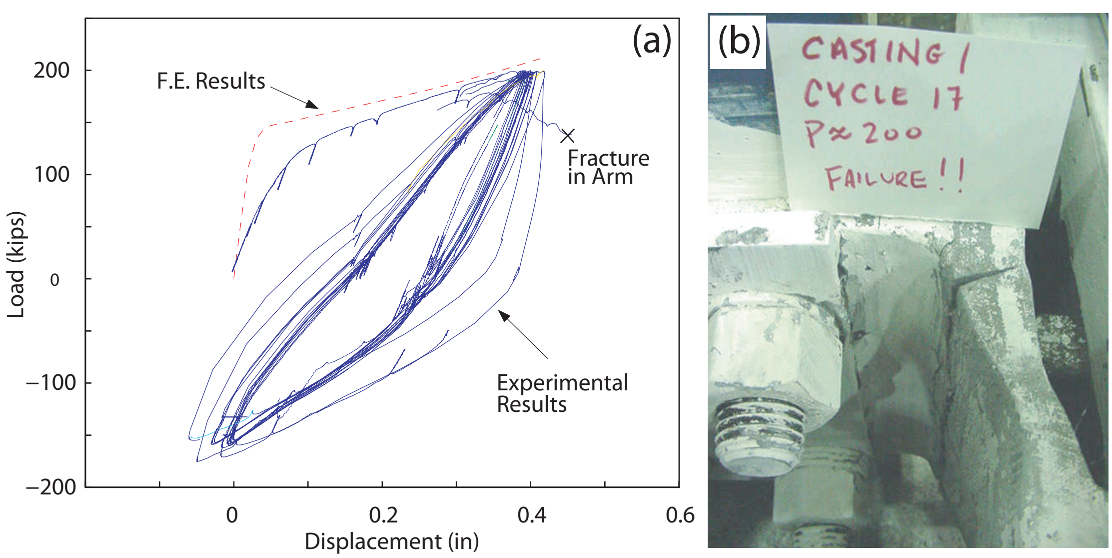

Fig. 9. Alpha prototype experiment: (a) hysteresis curve; and (b) fracture of arm.

Catenary Action

The base end-region configuration will be shown to minimize bolt forces in the MC (Sumer et al., 2007). However, the high stiffness it provides also causes catenary forces to develop in the MC arms at large ductility demand (Fleischman and Sumer, 2006). A catenary force is an axial tension force that builds up in a flexural member at large deflections due to its lengthening (see Figure 10a). Catenary effects were typically ignored for the ADAS device as it possessed boundary conditions at the device ends that provided some compliance to axial deformation (Whittaker et al., 1989). It was noted these forces in the ADAS should still be accounted for at large displacement levels; they were compensated for in the experimental loading (Alonso, Bertero, and Astaneh, 1989). For the MC application, however, where compliance to axial deformation would translate directly into rigid body rotation of the beam at the column connection, high axial stiffness is desirable, and thus rather than avoid catenary force, the goal is simply to create a form that can accommodate it.

As the arm deflects, the relationship between the local shear, axial force and moment acting on a section change due to the orientation (see Figure 10a). This action is termed geometric nonlinearity. It is noted that later equations will be based on the catenary force at the arm terminus, *N*, which is parallel to the column face. Since the MC arm is intended to serve as the source of energy dissipation in a seismic event, material nonlinearity is also involved. The MC arm yield state is dependent on all three force components at a section: moment, shear, and axial force (Fleischman and Sumer, 2006).

Accordingly, the element constitutive relationships in the finite element analyses for developing the MC prototype utilize material plasticity and large deformation capabilities. The distributed plasticity formulation inherent in the solid model is appropriate for capturing shear/flexure modes present in the arms. The material model for monotonic loading employs multi-linear kinematic hardening principles, the von Mises yield function, and the Prandtl-Reuss flow equation (ANSYS, 2003). Mild steel stress-strain curves are reproduced from uniaxial tension tests for the cast steel and converted into detailed piecewise-linear true stress/logarithmic strain relationships for large deformation analysis (see Figure 10b). For the monotonic analyses, the formation of a ductile crack (Kuwamura and Yamamoto, 1997) was assumed when the (true) strain reached a critical strain value (indicated in Figure 10b), taken as the ultimate true strain value of 0.285 (Fleischman and Sumer, 2006) from the foundry mechanical testing of the cast material. This approach for the prototype development, albeit approximate, is subsequently validated in experiments (Sumer et al., 2007).

ANALYTICAL DEVELOPMENT OF MC BETA PROTOTYPE

The development of the MC Beta prototype configuration shown in Figure 1 centered on two analytical investigations: (1) determination of optimum arm geometry, and (2) evaluation of end-region alternatives. These investigations are summarized here and design expressions are provided. It is noted that a detailed description of the former appears in (Fleischman and Sumer, 2006). The analytical studies were

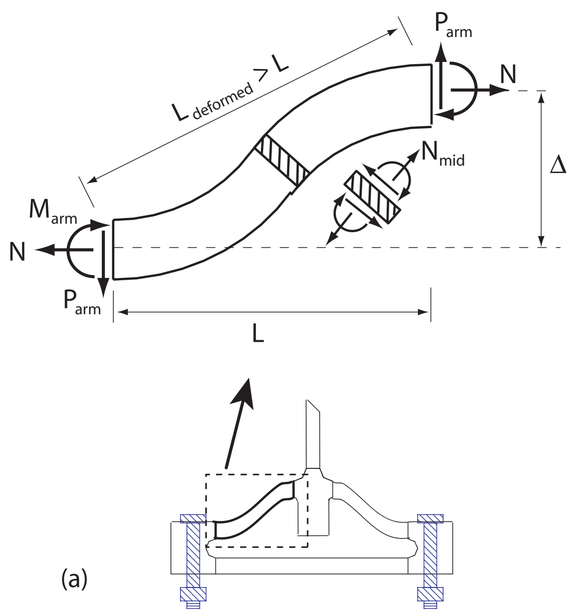

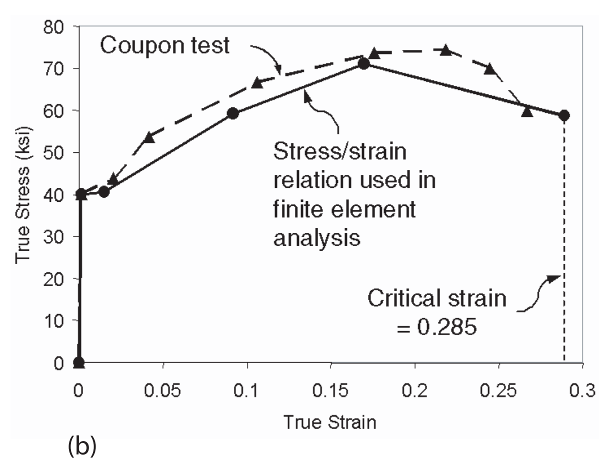

Fig. 10. (a) Catenary action; (b) stress-strain curves for cast steel.

performed under monotonic loading conditions. Once the prototype configuration was established, the design was validated (analytically and experimentally) under cyclic loading conditions (Sumer et al., 2007).

Determination of Optimum Arm Geometry

Arm geometry is described by four main geometric parameters as indicated in Figure 11a: (a) maximum nominal width, B_{max}, at the end of the arm; (b) minimum width, B_{min}, at the middle of the arm; (c) length of the arm, L; and, (d) arm thickness, t. Fillets transition the constant width mid-region to secants between opposing ends of the maximum nominal width (these secants make an X-shape) and also at the end of the arms.

Optimum arm geometry (in terms of minimizing plastic strain demand) is defined through the following geometric ratios identified in parametric studies (Fleischman and Sumer, 2006) and shown in Figure 11b:

a. A percentage width reduction $B_{min}/B_{max} = 0.45$.

b. An aspect ratio $L/B_{max} = 2$.

c. A limiting length-to-thickness ratio $L/t > 4$.

d. A fillet radius $r_0 = 10/L$ (where r_0, L are in in.).

To illustrate the effect of width reduction, consider a comparison between the MC arm (using the optimum geometry of Figure 11b), a constant width plate (representing a traditional connection detail piece such as the flange of a WT section), and an ADAS element. Results are shown for half-symmetry representations of single arm elements using a fine-mesh 3D-FE model (see Figure 12c). The elements are the same length and share the same maximum width. At the "useful limit" displacement (corresponding to 0.05 radian), concentration of plastic strain is observed at the ends of the constant width plate as a result of the plastic hinges forming due to reverse curvature bending (see WT in Figure 12b and 12c). As a result, the strains in this region are beyond the previously defined "critical" strain of 0.285. The ADAS geometry eliminates the concentrated plastic hinges as has been well documented (see Background). However, the ADAS shape develops a strain concentration at the minimum section (see ADAS in Figure 12b and 12c). The reason for this concentration, analogous to "necking" of a tensile coupon, is the development of catenary forces. The critical strain was exceeded for the ADAS at a connection rotation of 0.022 radian. In contrast, the MC geometry produces a relatively uniform plastic distribution along the arm (see MC in Figure 12c) and is at all locations below the critical strain (see Figure 12b).

Another key geometric ratio is the arm aspect ratio (L/B_{max}). Figure 13 shows plastic strain versus arm aspect ratio at 0.05 radian for three arm lengths. As seen, the strain demands become insensitive to this parameter at aspect ratios greater than 2. However, the plastic strain demand grows rapidly as the arm becomes squatter (this response explains why the MC employs a series of parallel arms rather than a single bending element). As shown by the schematics in Figure 13, the greater the aspect ratio, the more parallel arms fit on a given connector width, and thus the less practical the casting (more expensive tooling required). This condition dictates use of the lowest aspect ratio that still minimizes strain demand, in other words, $L/B_{max} = 2$.

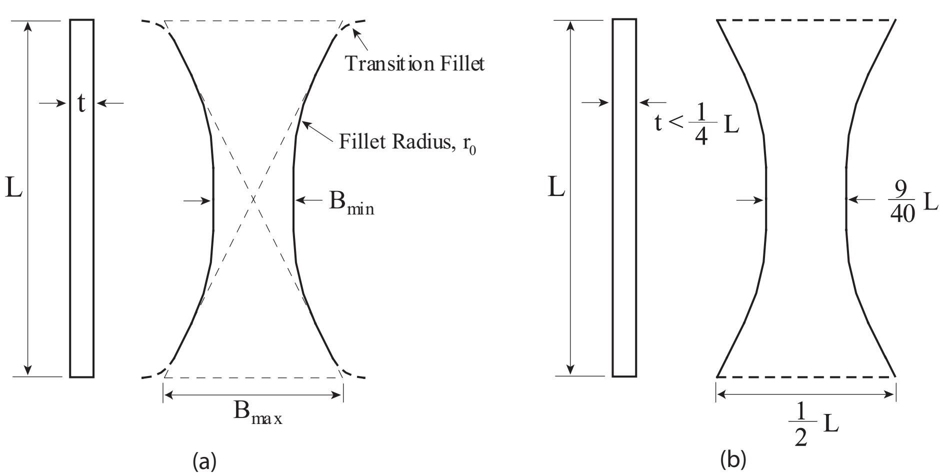

Fig. 11. MC Beta arm geometry: (a) geometric parameters; (b) optimum ratios (after Fleischman and Sumer, 2006).

The remaining requirements of the length-to-thickness limit and the radius size are needed to avoid a less ductile shear/flexure mechanism exhibited by thicker arms and strain concentrations in the transition regions, respectively (Fleischman and Sumer, 2006). The uniform strain response shown in Figure 12b is representative of all MCs of practical length provided they possess these optimum ratios. With optimum geometry established, MC design quantities can be developed.

MC Design Quantities

Design expressions (strength, stiffness, and ductility) are presented here for MC arms possessing the optimized geometric ratios. The expressions are semi-rational, in other words, based on classical formulas but calibrated to finite element parametric studies. The strength and stiffness values for a single arm are converted into design quantities for the entire MC by multiplying by the number of arms, *n*. All units are in kips and inches.

Figure 14a shows a schematic of the load-deflection for an isolated MC with the key design quantities indicated. The MC yield strength, P_y, is controlled by a flexural mechanism forming in the arms under double curvature (Fleischman and Sumer, 2006). For a single arm, the classical plastic mechanism [see inset (i) in Figure 14a] is

$$\frac{2M_p^{arm}}{L}$$

where

$$M_p^{arm} = F_y Z^{arm}$$

$$Z^{arm} = \tfrac{1}{4} B_{max} t^2$$

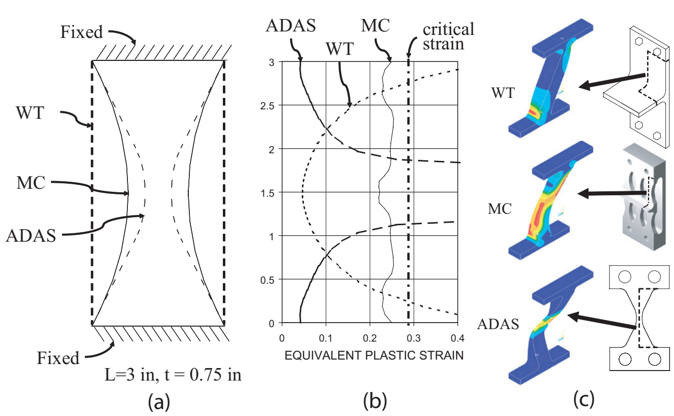

Fig. 12. Distribution of equivalent plastic strain in plate, MC arm and ADAS (0.05 radian) (after Fleischman and Sumer, 2006).

Substituting the optimized geometry for *n* arms gives

$$P_y = 0.23 n F_y t^2 \tag{1}$$

where a calibration factor of 0.9 has been introduced to match the finite element analyses (see Figure 15a). Similarly, the classical solution for the stiffness of a fixed-guided beam of

$$\frac{12EI_{eff}^{arm}}{L^3}$$

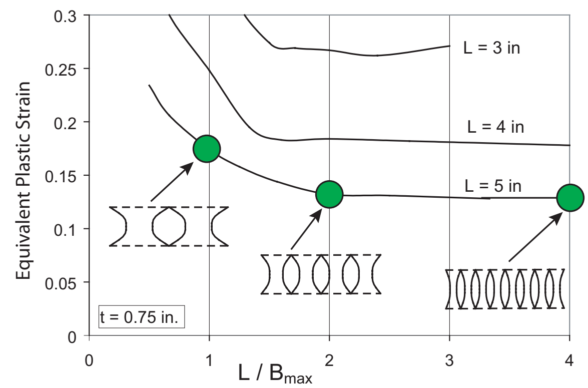

Fig. 13. Strain demand vs. aspect ratio (after Fleischman and Sumer, 2006).

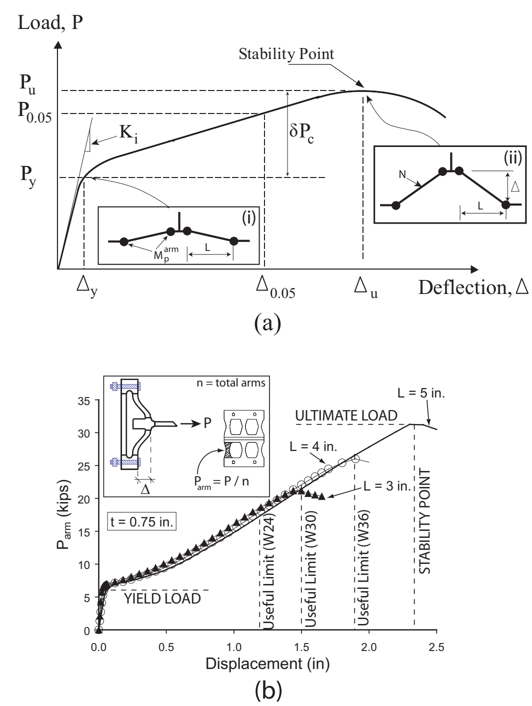

Fig. 14. (a) Design quantities for (isolated) MC; (b) stability point vs. arm length.

leads to a MC initial stiffness K_i of

$$K_i = 5782n\frac{t^3}{L^2} \tag{2}$$

where

$$I_{eff}^{arm} = \frac{1}{12}\left(\frac{B_{max}}{2}\right)t^3$$

A calibration factor of 0.8 is used in Equation 2 to match the finite element results (see Figure 15b).

It is noted that the optimum geometry, expressed as ratios, essentially relates the design quantities to a single geometric parameter. Arm length, L, is the reasonable choice for this independent variable. For convenience, the design quantities in Equations 1 and 2 have been expressed both in terms of L and t, since the L/t ratio of 4 is only a lower limit, and thus this exact relationship may not hold for all designs. Nevertheless, it is useful to examine the effect of this independent parameter L on the MC response.

Figure 14b shows the load-deflection response (for individual arms, not the entire connector) for three arms of the same thickness but of differing length, and each possessing the optimized geometric ratios as shown in Figure 11b. It may seem counterintuitive that a longer arm of identical thickness would possess the same yield strength; however, the section width also increases to keep the optimum geometry (this explains why L does not appear in Equation 1). Thus, the reduction in strength from a longer arm span is balanced by the wider arm cross-section. However, fewer parallel arms will be able to fit the available geometry of the column face. Therefore, while the individual arm strength stays constant, the overall MC yield strength (and stiffness) will decrease as the arm lengthens (for a given thickness), since the number of arms, n, able to fit the available column face decreases.

The benefits of increasing MC strength and stiffness through the use of shorter arm lengths are, however, offset by two factors: (1) ductility capacity and (2) onset of the stability point. For the former, an efficiency measure (arm strength relative to plastic strain demand) was shown to increase with arm length (Fleischman and Sumer, 2006); in other words, the gain in strength of a shorter arm is exceeded by the loss in ductility. Consideration of the latter, stability point, requires further examination of the MC arm response as discussed next.

The curves in Figure 14b exhibit a significant overstrength (P_u/P_y). The reason for this overstrength is the development of catenary action. The catenary forces augment the maximum force possible from a plastic mechanism only. The maximum catenary force possible is controlled by the minimum cross-section in the MC arm, $A_{min} = B_{min}t$ (see Figure 11a), and accordingly the largest catenary force that can be supported is $N_{mid,u} = B_{min}tF_u$, which in terms of the optimum

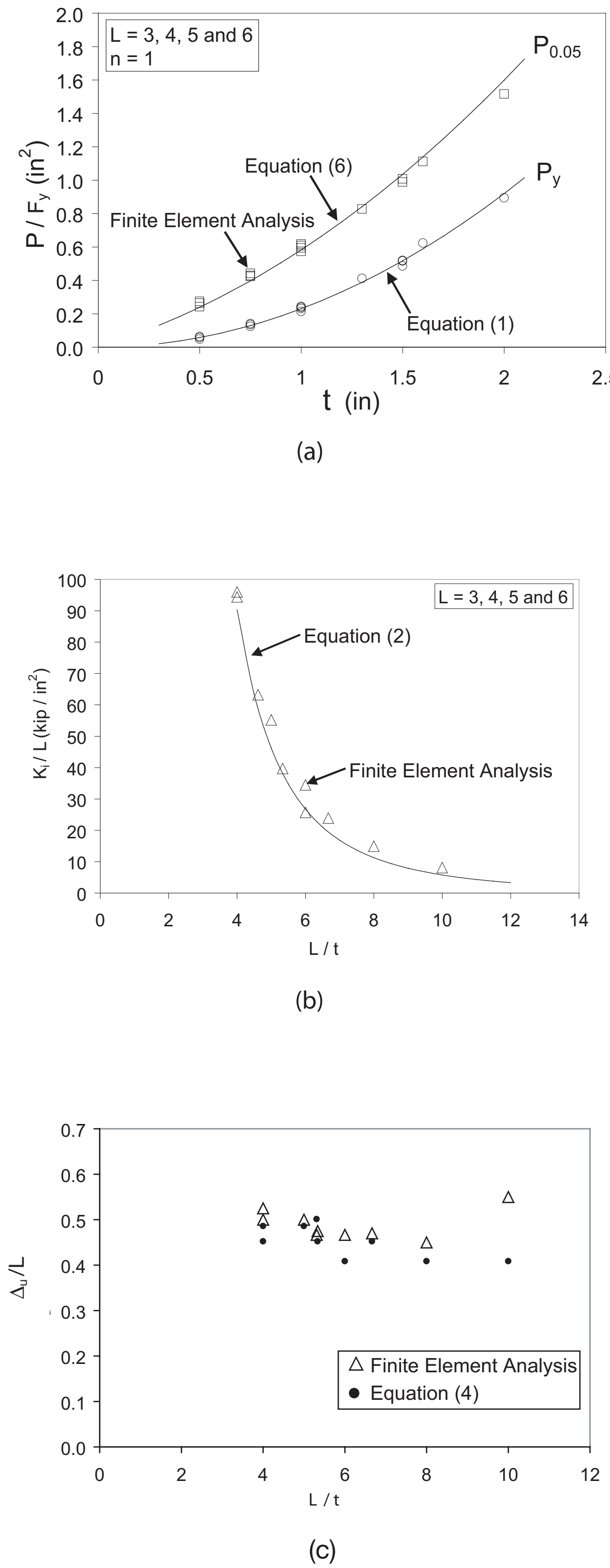

Fig. 15. MC design parameters: (a) load; (b) initial stiffness; (c) stability point.

geometry is, for a single MC arm,

$$N_{mid,u} = 0.203LtF_u \tag{3}$$

where a finite element calibration factor of 0.904 has been applied. Attainment of this catenary force corresponds to the achievement of P_u for the connector. Accordingly, the deflection at P_u is termed a stability point since once achieved, the MC arm undergoes a "necking" mechanism at its minimum arm cross-section. This is the same mechanism exhibited by the ADAS in Figure 12c, thus the MC arm geometry delays rather than eliminates this behavior. The following empirical expression was developed for the stability point deflection (see Figure 15c),

$$\Delta_u = 0.486Lt^{0.25} \tag{4}$$

Using this value, a simple kinematic relationship transforms the maximum catenary force into an increment of load on the connector, which is added to the yield load to produce the MC ultimate strength,

$$P_u = P_y + \delta P_c \tag{5a}$$

where δP_c is the increment of load mainly due to catenary forces. Equation 5a can be rewritten as

$$P_u = P_y + 0.92nN_{mid,u}\left[\sin\left[\tan^{-1}\left(\frac{\Delta_u}{L}\right)\right]\right] \tag{5b}$$

where 0.92 is the finite element analysis calibration factor and the term in brackets is the simple transformation based on a truss analogy at the secant angle [see inset (ii) in Figure 14a] that accounts for the fact that N_{mid} acts at an angle (refer to Figure 10a). Insertion of Equations 3 and 4 into Equation 5b and evaluation of the trigonometric expressions yields

$$P_u = P_y + 0.091nLF_uC_{t1} \tag{5c}$$

where C_{t1} expresses the effect of thickness on the overstrength,

$$C_{t1} = \frac{2(t)^{5/4}}{\sqrt{4+\sqrt{t}}} \cong 1.06t - 0.16 \tag{5d}$$

The ultimate load value can be referenced back to the strength at the "useful" rotation $P_{0.05}$ (indicated schematically in Figure 14a), approximated using a straight-line interpolation,

$$P_{0.05} = P_y + \left[\frac{\Delta_{0.05}}{\Delta_u}\left(P_u - P_y\right)\right] \tag{6}$$

The accuracy of the design equation is shown in Figure 15a.

The design intent dictates that the MC arm must be long enough to prevent the stability point from occurring within expected beam rotation demands. The deflections corresponding to "useful" rotations are indicated for 24-, 30-, and 36-in.-deep beams in Figure 14b, implying a MC arm length requirement of approximately $L > d_{bm}/8$ for the cases shown, though modified through a factor of safety to $L > d_{bm}/6.5$ in the prototyping (Sumer et al., 2007). The use of longer arms dictates that arm thickness should remain reasonably near the allowable upper limit ($t = L/4$) in the interest of maximizing strength and stiffness, as well as for castability (Sumer et al., 2007). The need for longer arm elements also leads to the next step in the concept development: creating a bolted connector with sufficiently long flexural spans that does not suffer adverse performance due to bolt prying.

Evaluation of End-Regions

The use of a cast configuration permits the consideration of nontraditional shapes for the areas where the connector is bolted. The primary objective in selecting a shape for these "end-regions" is to minimize the high prying forces and moments that would otherwise occur in bolts at longer gages. The end-region can also provide a stiff boundary for the arms. Four possible end-region configurations were considered: MC-NoBase, MC Beta, MC-Outrigger, and MC-Eccentric (see Figure 16). The MC-NoBase configuration (end-region with no added features) is simply used as a control to compare the MC directly to a WT, thus allowing the effects of the arms to be isolated. The MC Beta configuration contains a back piece (or base) that connects each end-region and, as will be described, was the eventual choice for the MC Beta prototype. The MC-Outrigger configuration employs an extended outer bearing pad that increases the leverage of the contact region. The MC-Eccentric configuration has an end-region that contains secondary bolts eccentric to the main bolts. Note that for each configuration, an element at the junction of the arms protrudes to the back of the connector. This feature, termed a compression pad, is provided to transmit the beam flange compressive loads directly to the column as the MC cycles between tension and compression loading during seismic response.

In order to evaluate the end-region configurations, a 2D-FE model was created representing a tributary cross-section of the MC. Figure 17 shows the 2D-FE model in half-symmetry representation about the stem. It is noted that this is the scaled MC Beta used in the experimental program (Sumer et al., 2007).

The 2D-FE MC model is a plane-stress representation of a single arm of the MC with a scaled representation of the bolt. Plane-stress quadrilateral elements represent the angle and bolt; point-to-point pseudo-elements capture contact between the MC, the bolt and the column flange. The load is applied via displacement control at the MC stem. The models include material and geometric nonlinearity, the latter due to changing contact surface and catenary action at large deflection. The aspects of bolt behavior captured in the model include preload, slip, bearing, axial/rotational flexibility, nonuniform pressure distributions, and fastener inelasticity. Evaluation of several designs, as required in developmental research, was facilitated by the parametric design language and adaptive meshing features of the commercial software ANSYS (ANSYS, 2003).

The end-region alternatives were conceived with consideration of prying effects only. However, catenary forces were also found to affect bolt performance. Thus, prior to discussing the reduction of prying forces, the effect of catenary forces on the bolts is presented. To illustrate this, consider Figure 18, which shows load versus deflection at the MC stem and catenary force versus deflection for two end-region alternatives: MC Beta (with a base) and MC-NoBase (without a base). The two connectors exhibit nearly identical overall load-displacement behavior and catenary force development into the post-yield regime. However, at approximately 0.7 in. deflection, within the useful displacement range, bolt slip (due to the catenary force) occurs for the MC-NoBase. Though the overall load-displacement response (see Figure 18a) does not change significantly, the catenary force (see Figure 18b) in the MC-NoBase levels off while the MC Beta continues to carry increasing catenary force (due to a self-equilibrating force in the base as will be shown later). Once the MC-NoBase bolts slip into bearing, the catenary force increase resumes, but is now transferred as direct shear in the bolt rather than through the friction. Thus, the MC-NoBase under tension is susceptible to a bolt shear failure. Among the end-region alternatives considered, all seemingly effective in resisting traditional prying, only the base end-region fully protects the bolts from catenary-action shear loading (the MC-Eccentric provides reasonable protection but was abandoned due to the difficulty associated with the extra bolting). Therefore, the base feature was selected as the MC end-region configuration. Accordingly, the discussion of prying mitigation to follow will be restricted to this configuration.

The equilibrium condition in Figure 19b for a traditional flange connection results in a bolt force amplified by a prying force Q; and a moment Qa that must be resisted by the section at the bolt line. The goal of the MC end-region configuration is to minimize or eliminate the prying force Q to avoid an axial failure in the bolt threads (due to Q) or a flexural failure in the bolt shank (due to Qa). Also required, and not fully appreciated at the outset of the study, was the need for redirecting the catenary force to avoid a bolt shear failure. For the MC Beta end region (Figure 19a), both these objectives are accomplished through the development of self-equilibrating forces in the base. The component of the catenary force parallel to the base creates tension at the end of the arm (N). This tension force is equilibrated by an (essentially) equal and opposite compression force in the base (for convenience, one arm is assumed tributary to one bolt for this schematic). The couple established by these forces (acting at an arm/base separation s) can equilibrate the couple created by the eccentrically applied arm shear (equal to P_{arm} acting at a distance e) with the total bolt reaction (T_B-C) without the presence of a prying force. This is clearly impossible for the traditional WT (see Figure 19b).

To account for the full equilibrium condition, finite element analyses of the half-symmetry model shown in Figure 17 were examined varying the parameters e and s (as indicated in Figure 19a), where e and s refer to bolt-to-arm eccentricity and arm-base separation distances, respectively. In the analyses, the bolts (⅞ in., ASTM A325) have been selected such that their factored tension strength (and hence their initial pretension) (AISC, 2001) is slightly greater than the MC ultimate load, P_u.

Figure 20 shows a schematic for the different prying conditions obtained in the analyses. As may be expected, when

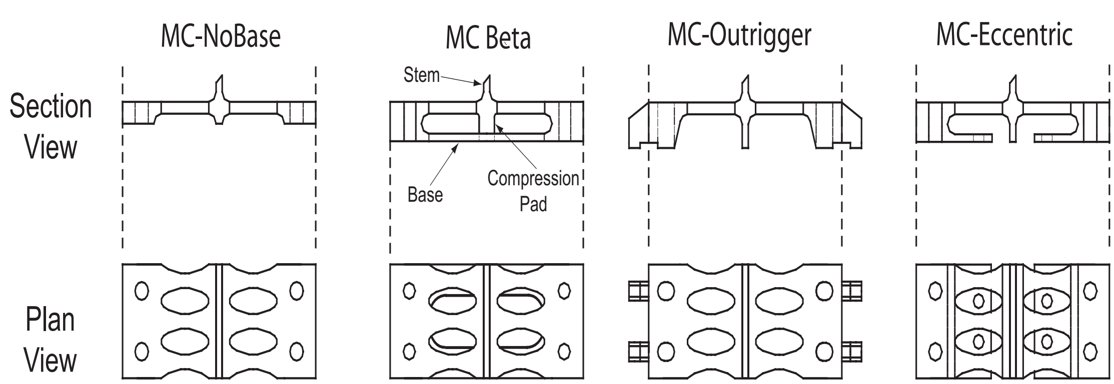

Fig. 16. End-region configurations considered during the development process.

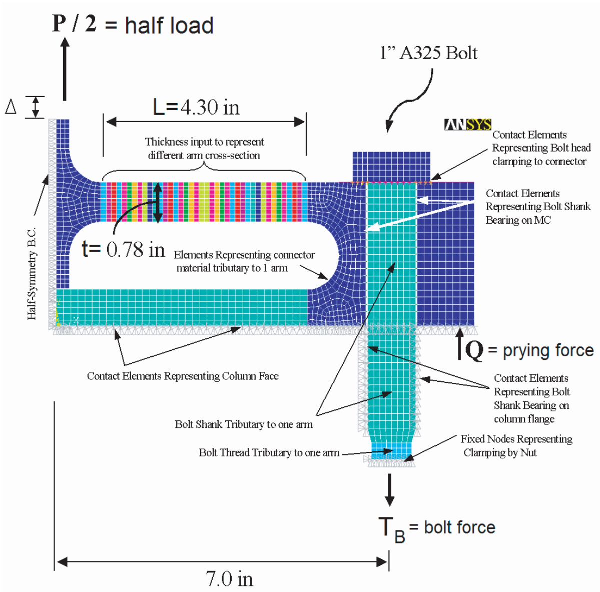

Fig.17. 2D half-symmetry model of scaled MC Beta.

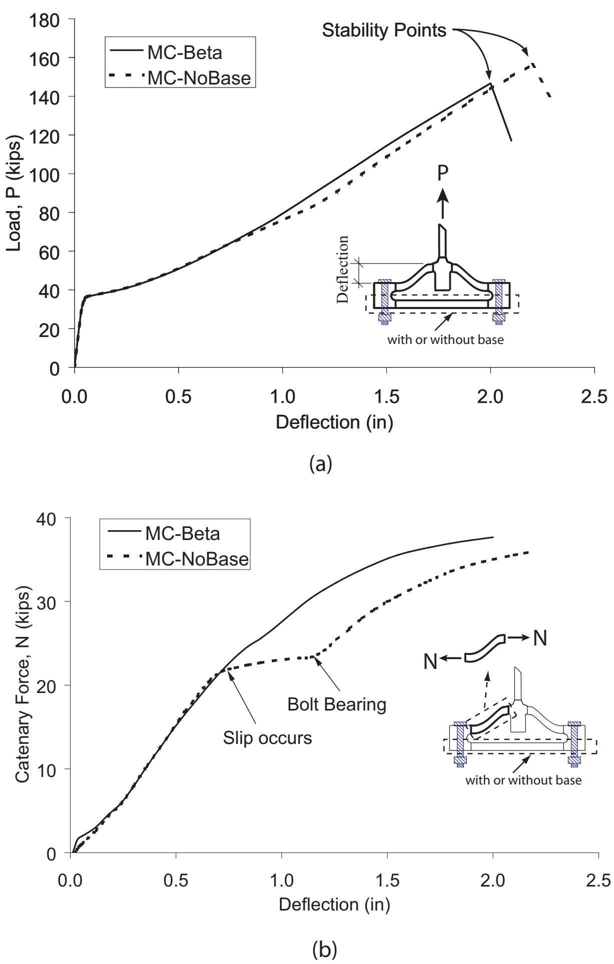

Fig. 18. MC Beta end-region alternatives: (a) load vs. deflection, (b) catenary force.

e becomes large with respect to s (Figure 20a, top) or s small with respect to e (Figure 20b, bottom), prying forces develop. Interestingly, if the opposite situation exists, in other words, e small with respect to s (Figure 20a, bottom) or s large with respect to e (Figure 20b, top), the contact condition migrates to a position inside the bolt gage. These outcomes imply a critical combination of e and s exists at which contact occurs at the bolt line only, and hence prying is eliminated. This condition was produced in the analyses (see Figures 21a and 21b). The free body diagram of Figure 19a is used to illustrate the determination of this optimum end region geometry, as follows.

The FE analyses indicated that the base lifts off the column flange surface between the end regions (see Figure 19a). With no contact occurring between the base and column flange, the shear in the base (V_{base}) is zero. Further, the analyses indicate that the moment at the end of the base (M_{base}) is negligible for a clamped condition (in other words, bolt pretension not overcome). Thus the resulting equilibrium relationship (per arm) is

$$N \times s - M_{arm} \cong P_{arm} \times e \tag{7}$$

where N is the catenary force at the arm terminus (parallel to base). A relationship for dimensions e and s can be developed by evaluating Equation 7 at ultimate, $P_{arm} = P_u / n$. The catenary force component parallel to the base at ultimate, $N = N_u$, is the horizontal component of $N_{mid,u}$, expressed here based on the middle section orientation (Fleischman and Sumer, 2006) as shown in Figure 10a,

$$N_u = N_{mid,u}\left[\cos\left(1.5\tan^{-1}\left(\frac{\Delta_u}{L}\right)\right)\right] \tag{8a}$$

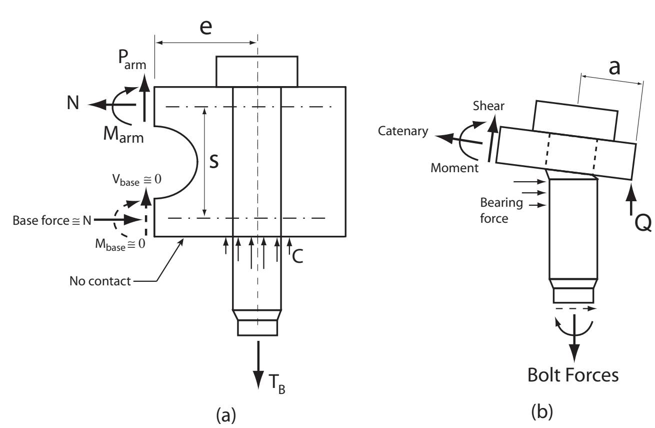

Fig. 19. Equilibrium condition at bolt: (a) MC end-region (per arm); (b) WT.

After substitution of Equations 3 and 4 into Equation 8a, and simplification of the trigonometric expression, Equation 8a becomes

$$N_u = 0.179 L F_u C_{t2} \tag{8b}$$

where C_{t2} expresses the effect of thickness on the horizontal force component at ultimate

$$C_{t2} = \frac{2t}{\sqrt{4+\sqrt{t}}} \cong 0.85t - 0.04 \tag{8c}$$

The arm end moment, M_{arm}, is approximated using a section plastic moment including strain hardening, but reduced for the presence of axial load, as determined in (Fleischman and Sumer, 2006), and in terms of the optimum geometry is

$$M_{arm} \cong 0.15 L t^2 F_y \tag{9}$$

In this way, a relationship can be established for the design parameters s and e that minimizes Q (in other words, $Q \rightarrow 0$).

$$2s - t = \left(1.5\frac{t}{L} + 1\right)e \tag{10}$$

where e and s are in inches. Clearly a desire exists to minimize s for practical reasons related to terminating the beam near the column face and minimizing e for fitting a web connection between the modular connectors. Thus, the value of s is selected just large enough to provide the needed separation between the arm and base for castability requirements, as is described in Sumer et al. (2007).

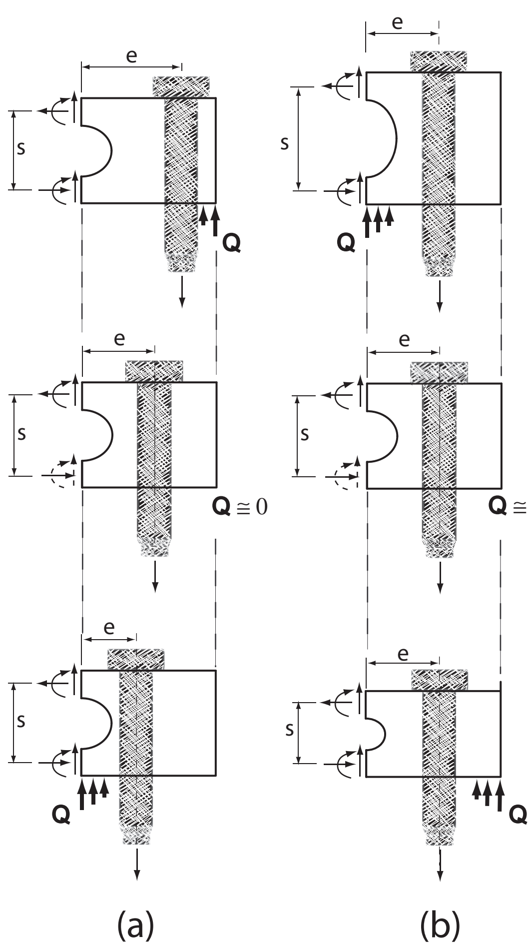

Fig. 20. End-region study: (a) bolt eccentricity varied; (b) gap varied.

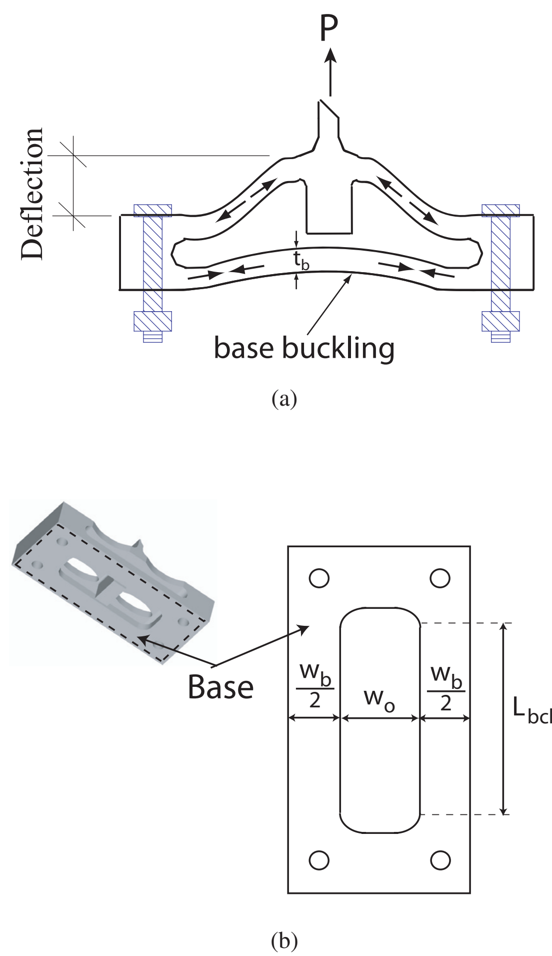

Fig. 21. (a) Base buckling; (b) base parameters.

The elimination of prying allows the bolts to be sized for direct tension. Using capacity design concepts, this value should be based on the largest direct tension that can develop in the MC, in other words

$$\phi R_n > \frac{P_u}{n_b} \tag{11}$$

where

R_n = $F_t A_b$ (AISC, 2001) is the nominal bolt tension strength

n_b = number of bolts in the MC

ϕ = 0.75 is the strength reduction factor

It should be noted that for fully pretensioned bolts this provides an initial total clamping force roughly equivalent to P_u.

Design of Base

The base itself must be designed to transfer the forces shown in Figure 19a without yielding or buckling. The relative slenderness of the base element on either side of the opening dictates buckling as a possible limit state (see Figure 21a). Accordingly, for the base geometry selected for castability (Sumer et al., 2007), a base clear length, L_{bcl}, and a base element width of $w_b = nB_{max} - w_0$ (see Figure 21b), the elastic buckling load is approximated (for a conservatively assumed pinned end condition) as $P_{bcl} = \pi^2 EI/(L_{bcl})^2$. Given that the base force contribution per arm on one side is essentially equal to N (see Figure 19a), the maximum compressive axial force demand in the base can be expressed by Equation 8 multiplied by $n/2$, rendering the base geometry requirements for the limit state of buckling and yielding as

$$\frac{w_b (t_b)^3}{(L_{bcl})^2} > \frac{n}{2}\left(\frac{12N_u}{\pi^2 E}\right) \tag{12a}$$

and

$$w_b t_b F_y > \frac{n}{2}(N_u) \tag{12b}$$

respectively. Recognizing that the base dimensions must follow certain relationships, namely $L_{bcl} \cong 2.5L$ and $W_{MC} \cong 1.2nL/4$, where in each case the relationship is approximate due to the presence of fillet radii, and since it will be shown (Sumer et al., 2007) that $w_0 \cong 0.43W_{MC}$ for castability renders $w_b \cong 0.16nL$. Inserting these approximations as well as Equation 8b into Equations 12a and 12b provides the design equation for the base thickness,

$$t_b > \max\left[\sqrt[3]{\frac{4.25C_{t2}L^2F_u}{E}}, \frac{0.52C_{t2}F_u}{F_y},\ 0.75\right] \tag{13}$$

where a factor of safety is taken as 1.25 in the design of the MC prototype.

CONCLUSIONS

A bolted cast modular connector, the MC, has been conceived and developed into a (Beta) prototype design through an extensive analytical program. The potential for reliable and highly ductile performance of the MC is a product of two features easily cast: (1) variable section arms that spread the plastic zone thus eliminating strain concentrations, and (2) a stiff end-region connected by a base that eliminates prying action and shear force due to catenary action on the bolts. The latter feature permits the arms to be sufficiently long to produce outstanding ductility without a concern for bolt failure. Instead, the bolts for the MC are to be designed for only direct tension.

Design expressions and geometric properties have been provided here for the MC Beta prototype. The prototyping and experimental verification of the MC Beta prototype is described in the companion paper (Sumer et al., 2007).

ACKNOWLEDGMENTS

This research was supported by NSF CAREER Award Grant CMS-01-96120. Supplemental funds were provided by AISC and SFSA member company Varicast, Inc. The computer laboratory was provided through a grant from Intel, Inc., and the finite element software was donated by industry partner Swanson, Inc. (ANSYS). The authors are grateful for this support.

Any opinions, findings, and conclusions or recommendations expressed in this material are those of the author(s) and do not necessarily reflect the views of the National Science Foundation.

NOMENCLATURE

a = distance between center of bolt and edge of flange

B_{max} = maximum width of MC arm

B_{min} = minimum width of MC arm

C = clamping force

C_{bm} = compression force in beam flange

C_0 = initial clamping force due to bolt pretensioning

d_{bm} = depth of beam

e = distance between center of bolt and MC arm

E = Young's modulus of steel

F_y = yield stress

F_u = ultimate stress

I_{eff}^{arm} = effective moment of inertia of MC arm about weak axis

K_i = initial stiffness of entire MC Beta

L = length of MC arm

L_{bcl} = base element length

M_{arm} = MC arm bending moment

M_{base} = MC base bending moment

M_{bm} = beam bending moment

M_p^{arm} = MC arm bending moment at ultimate

N = catenary force acting on arm section

$N_{mid,u}$ = catenary force in the middle of the MC arm at ultimate

n = number of MC arms

n_b = number of bolts in MC Beta

P = beam flange force tributary to entire Modular Connector

P_{arm} = beam flange force tributary to one arm

P_{bcl} = base element elastic buckling load

P_y = yield load of entire Modular Connector

P_u = ultimate load of entire Modular Connector

$P_{0.05}$ = load of entire Modular Connector at 0.05 rad connection rotation

Q = prying force

R_n = nominal bolt strength

r_0 = fillet radius of MC arm

s = distance between MC arm and MC base (from center-to-center)

t, t_b = MC arm thickness, base thickness

T_{bm} = tension force in beam flange

T_B = bolt force

T_{B0} = bolt pretensioning force

V_{base} = shear force acting on MC base

V_{bm} = beam shear force

w_b = base element width

Z^{arm} = MC arm plastic modulus

δP_c = increment of load due to catenary forces

Δ = MC arm transverse displacement

Δ_u = stability point

$\Delta_{0.05}$ = useful limit

θ_{conn} = beam end relative rotation

REFERENCES

Aiken, I.D., Nims, D.K., Whittaker, A.S., and James M.K. (1993), "Testing of Passive Energy Dissipation Systems," *Earthquake Spectra*, Vol. 9, No.3, Earthquake Engineering Research Institute, CA.

Alonso, J., Bertero, V.V., and Astaneh, H. (1989), "Mechanical Characteristics of X-Plate Energy Dissipators," CE-299 Report, University of California, Berkeley, CA.

AISC (2001), *Load and Resistance Factor Design Manual of Steel Construction*, 3rd Ed., American Institute of Steel Construction, Inc., Chicago, IL.

AISC (2005), *Seismic Provisions for Structural Steel Buildings*, March 9, American Institute of Steel Construction, Inc., Chicago, IL.

ANSYS (2003), "Elements and Theory Reference," Version 8.0, 9th Ed., SAS IP, Inc.

Astaneh, A. (1995), "Post-Earthquake Stability of Steel Moment Frames with Damaged Connections, Connections in Steel Structures III, Behavior, Strength and Design," *Proceedings of the Third International Workshop*, Trento, Italy, pp. 391.

Bergman, D.M. and Goel, S.C. (1987), "Evaluation of Cyclic Testing of Steel-Plate Devices for Added Damping and Stiffness," Report UMCE87-10, Department of Civil Engineering, University of Michigan, Ann Arbor, MI.

FEMA (1999), "Interim Guidelines Advisory No. 2 Supplement to FEMA-267," FEMA 267B, prepared by the SAC Joint Venture for the Federal Emergency Management Agency, Washington, DC.

FEMA (2000), "Recommended Seismic Design Criteria for New Steel Moment-Frame Buildings," FEMA 350, prepared by the SAC Joint Venture for the Federal Emergency Management Agency, Washington, DC.

FEMA (2000), "State of the Art Report on Connection Performance," FEMA 355D, prepared by the SAC Joint Venture for the Federal Emergency Management Agency, Washington, DC.

Fleischman, R.B. and Hoskisson, B. (2000), "Development of Modular Connectors for Seismic Resistant Steel Moment Frames," Structures Congress, ASCE, Philadelphia, PA.

Fleischman, R.B., Sumer, A., and Li, X. (2002), "Development of Modular Connections for Steel Special Moment Frames," SFSA Technical & Operations Conf., Chicago, IL.

Fleischman, R.B. and Sumer, A. (2006), “Optimum Arm Geometry for Ductile Modular Connectors,” *Journal of Structural Engineering*, ASCE, Vol. 132, No. 5, pp. 705–716.

Hoskisson, B. (2000), “Modular Connectors For Steel Seismic Resistant Moment Frames,” MS thesis, Department of Civil Engineering and Geological Sciences, Notre Dame, IN.

Kuwamura, H. and Yamamoto, K. (1997), “Ductile Crack as Trigger of Brittle Fracture in Steel,” *Journal of Structural Engineering*, Vol. 123, No. 6, pp. 729–735.

Leon, R.T., Swanson, J.A., and Smallidge, J.M. (1999), “SAC Steel Project - Subtask 7.03: Results and Data CD,” Georgia Institute of Technology, Atlanta, GA.

Maison, B.F., Rex, C.O., Lindsey, S.D., and Kasai, K. (2000), “Performance of PR moment Frame Buildings in UBC Seismic Zones 3 and 4,” *Journal of Structural Engineering*, Vol. 126, No. 1, pp. 108–116.

Malley, J. (1998), “SAC Steel Project: Summary of Phase 1 Testing Investigation Results,” *Engineering Structures*, Vol. 20, No. 4–6, pp. 148–162.

Monroe, R. (1995), “Steel Castings,” *Proceedings*, 12th SFSA T&O Conference.

Nair, R.S., Birkemoe, P.C., and Munse, W.H. (1974), “High Strength Bolts Subject To Tension And Prying,” *Journal of the Struct Division*, ASCE, Vol. 100, No. 2, pp. 351–372.

Piluso, V., Faella, C., and Rizzano, G. (2001), “Ultimate Behavior of Bolted T-Stubs II: Model Validation,” *Journal of Structural Engineering*, Vol. 127, No. 6, pp. 694–704.

Popov, E.P. and Takhirov, S.M. (2002), “Bolted Large Seismic Steel Beam-to-Column Connections Part 1: Experimental Study,” *Engineering Structures*, Vol. 24, pp. 1523–1534.

Roeder, C.W., Leon, R.T., and Preece, F.R. (1994), “Strength, Stiffness and Ductility of Older Steel Structures Under Seismic Loading,” SGEM Report 94-4, Department of Civil Engineering, University of Washington, Seattle, WA.

Steel Founders’ Society of America (1995), “Steel Castings Handbook,” 6th Ed., ASM International, Materials Park, OH.

Steimer, S.F., Godden, W.G., and Kelly, J.M. (1981), “Experimental Behavior of a Spatial Piping System with Steel Energy Absorbers Subjected to a Simulated Differential Seismic Input Report, UCB/EERC-81/09,” Earthquake Engineering Research Center, University of California, Berkeley, CA.

Steimer, S.F. and Chow, F.L. (1984), “Curved Plate Energy Absorbers for Earthquake Resistant Structures,” *Proceedings*, 8WCEE, San Francisco, CA.

Sumer, A. (2002), “Development of a Cast Modular Connector for Seismic-Resistant Steel Frames,” MS Thesis, University of Arizona.

Sumer, A., Fleischman R.B., and Palmer N. J., (2007), “Development of a Cast Modular Connector for Seismic-Resistant Steel Frames, Part 2: Experimental Verification,” *Engineering Journal*, AISC, Vol. 44, No. 3.

Swanson, J.A. and Leon, R.T. (2000), “Bolted Steel Connections: Tests on T-Stub Components,” *Journal of Structural Engineering*, ASCE, Vol. 126, No. 1, pp. 50–56.

Tyler, R.G. (1978), “Tapered Steel Cantilever Energy Absorbers,” Bulletin N.Z. National Society for Earthquake Engineering, Vol. 11, No. 4.

Varicast (2002), “Steel Casting Mechanical Testing Reports,” and transmittal.

Whittaker, A.S., Bertero, V.V., Thompson, C.L., and Alonso L.J. (1989), “Earthquake Simulator Testing of Steel Plate Added Damping and Stiffness Elements,” Report No. UCB/EERC-89/02, EERC, University of California at Berkeley, CA.